Additive Manufacturing 60 (2022) 103268

Contents lists available at ScienceDirect

Additive Manufacturing

journal homepage: www.elsevier.com/locate/addma

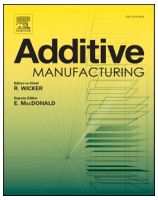

Material extrusion-based 3D printing for the fabrication of bacteria into functional biomaterials: The case study of ammonia removal application

Yan Li [a,b,c], Shuqiang Peng [a,e], Kunrong Li [a], Dan Qin [b], Zixiang Weng [a], Jiangwei Li [b], Longhui Zheng [a], Lixin Wu [a,*], Chang-Ping Yu [b,d,**]

[a] CAS Key Laboratory of Design and Assembly of Functional Nanostructures, Fujian Key Laboratory of Nanomaterial, Fujian Institute of Research on the Structure of Matter, Chinese Academy of Sciences, Fuzhou, Fujian 350002, China
[b] CAS Key Laboratory of Urban Pollutant Conversion, Institute of Urban Environment, Chinese Academy of Sciences, 1799 Jimei Road, Xiamen, Fujian 361021, China
[c] School of Ecological Environment and Urban Construction, Fujian University of Technology, Fuzhou, Fujian 350118, China
[d] Water Innovation, Low Carbon and Environmental Sustainability Research Center, National Taiwan University, Taipei 106, Taiwan
[e] University of Chinese Academy of Sciences, Beijing 100049, China

ARTICLE INFO

Keywords:
Material extrusion-based 3D printing
Heterotrophic bacteria
Dual crosslinking
Ammonia removal
Bio-ink

ABSTRACT

3D printing provides a new way of microbial immobilization technology and creates innovative designed bioactive structures containing microorganisms for remediation of environmental pollution. However, the bio-ink design remains a critical challenge due to the difficulty in creating a durable and bio-friendly material. Here, a novel dual-crosslinking PEGDA-Alginate-PVA-Nanoclay (PAPN) bio-ink containing one heterotrophic bacterium is reported for 3D printing functional biomaterial with the capabilities of ammonia removal. The results showed that PAPN 3D printed bio-scaffolds could effectively remove 96.2 ± 1.3% ammonia within 12 h, and the removal rate increased within repeated use owing to the growth of bacteria inside the bio-scaffolds. Preservation of the bio-scaffolds under room temperature without a culture medium for 168 h still maintained the microbial activity for ammonia removal. It is demonstrated that visible-light-based 3D printing procedures could maintain high cell viability for the majority of bacteria, and the porous structures of 3D bio-scaffolds could allow the permeability of nutrients for the growth of bacteria. This work demonstrates the potential of the dual crosslinked PAPN 3D bio-scaffold for the production and application of immobilized functional bacteria in wastewater treatment.

1. Introduction

Eutrophication in the water environment, caused by the excess discharge of nutrients i.e., nitrogen and phosphorus, is a global environmental problem [1,2]. It leads to algal blooms in the freshwater and marine ecosystems and affects human health and the quality of the environment [3,4]. Therefore, nitrogen removal from wastewater has gained increasing attention around the world [5]. Research has shown that bioaugmentation of functional microorganisms for removing target pollutants in the biological treatment processes could be an economical and eco-friendly way to improve the treatment performance [5–9]. To achieve long-term operational stability and easy recovery and reuse of the bioaugmented functional microorganisms in the biological system, microbial immobilization technology [8], referring to the restriction of cell mobility through chemical or physical means [9,10] has been developed. Nevertheless, microbial immobilization technology currently faces several challenges. For example, the previous preparation methods of immobilized microbial structures, such as sodium alginate in calcium chloride [11], polyvinyl alcohol (PVA) and sodium alginate in boric acid and calcium chloride [12], etc. were difficult to control shapes and three-dimensional structures with high surface area. In addition, the cellulose triacetate immobilization method, which can exhibit high mechanical strength, requires toxic solvents such as dichloroethane and toluene [13,14]. Therefore, developing novel methods to immobilize microorganisms with excellent performance is significant for advancing microbial immobilization technology in

* Corresponding author.
** Corresponding author at: CAS Key Laboratory of Urban Pollutant Conversion, Institute of Urban Environment, Chinese Academy of Sciences, 1799 Jimei Road, Xiamen, Fujian 361021, China.
E-mail addresses: lxwu@fjirsm.ac.cn (L. Wu), cpyu@iue.ac.cn (C.-P. Yu).

https://doi.org/10.1016/j.addma.2022.103268
Received 17 May 2022; Received in revised form 25 October 2022; Accepted 3 November 2022
Available online 9 November 2022

wastewater treatment.

In recent years, 3D printing technology has made substantial progress in printing orderly and complex porous structures [15–17]. 3D bioprinting uses computer design to achieve spatial assembly of different functional component materials and living cells, living bacteria, and other organisms into complex 3D active biomaterials, i.e., engineered living materials [18,19]. Recently, researchers have also begun to apply 3D bioprinting technology to the immobilization of microorganisms. Schaffner et al. [15] developed a functional ink called Flink, composed of hyaluronic acid, κ-carrageenan, and fumed silica. Bacteria were embedded in the hydrogel bio-ink through the pressure-driven printhead under UV (365 nm) crosslinking, and complex shapes were constructed, coupled with the metabolic capability of bacteria, to form functionally active biomaterials. In addition, Lehner et al. [20] developed a microbial 3D printing system that used bio-ink mixed with alginate and live bacteria. The study showed that *Escherichia coli* strains could be printed in multiple layers and remained viable for at least two days after the gel was formed. The research mentioned above demonstrated that it is feasible to use 3D bioprinting to make a bio-ink-based complex 3D bioactive structure as an alternative approach for the immobilizing microorganisms.

There are still several key issues in applying 3D bioprinting to immobilize microorganisms to make active microbial functional materials. First of all, the structure formed by 3D printing using bio-ink should entrap microorganisms and at the same time, allows the substrate to diffuse and therefore the development of bio-ink suitable for different types of microorganisms with excellent performance to meet various bioengineering applications is critical for microbial cell immobilization using 3D bioprinting. The choice of bio-ink compositions affects the viability of the immobilized microorganisms and further affects the efficiency of their application. The compositions of bio-ink should achieve good biocompatibility, suitable mechanical strength, decent biological and chemical stability. Second, the main components of hydrogel bio-ink are organic polymers, including natural polysaccharide and synthetic polymers. Natural polymers[21], such as collagen [22], gelatin [23], hyaluronic acid [21], and alginate [21], are generally nontoxic to organisms, with superior mass transfer performance, a mild operation process, and better cell growth compared with the synthetic materials [24]. However, they also have limitations, e.g., low mechanical strength and high biodegradability [21]. Synthetic polymer hydrogel materials, such as PVA, polyacrylamide, and water-soluble polyurethane, generally have higher mechanical strength and good chemical stability [25]. Adding nanomaterials to the polymer matrix is one of the strategies to effectively transfer loads and enhance the mechanical properties of hydrogels [26–29]. Lastly, to achieve long-term use of the 3D-printed microbial structures, the hydrogel must be crosslinked. The photoinitiator is excited by light irradiation and quickly generates free radicals, which can form a 3D network in a short time. However, the most commonly used water-soluble photoinitiator, Irgacure® 2959, has its maximum absorption wavelengths at 276 and 331 nm, which can cause certain damage to bacteria and other microorganisms and reduce their activity under prolonged irradiation. Thus, there is a need to use a photoinitiator with excellent biocompatibility, low toxicity, efficient absorption, and initiation under visible light for maintaining the activity of 3D-printed microbial structures.

Therefore, this study intends to develop novel compositions of hydrogel bio-ink with higher mechanical strength through different approaches, including the mixture of natural and synthetic polymers, a combination of photo- and calcium-crosslinking, and the addition of nanoparticles. In addition, to lower the potential impact on microbial activity, the photoinitiator with lower toxicity and effective initiation under visible light is applied in the bio-ink. An isolated heterotrophic bacterial strain, which can remove ammonia in the presence of organic carbon sources, is used to test the microbial function of the 3D-printed microbial structures. Successful application of microbial immobilization technology needs suitable materials and professional production techniques. The results obtained in this study can advance the development of microbial immobilization technology using 3D bioprinting and are beneficial for applying bioaugmentation in biological wastewater treatment processes.

2. Materials and methods

2.1. Materials and reagent

Sodium alginate (Viscosity 200 ± 20 mPa.s, CAS: 9005–38–3), Poly (vinyl alcohol) 1788 (PVA, alcoholysis 87–89%, CAS: 9002–89–5) were purchased from Sigma Aldrich, USA. 2,2′-Azobis[2-methyl-*n*-(2-hydroxyethyl) propionamide] (VA-086, 98%, CAS: 61551–69–7, Heowns), Poly(ethylene glycol) diacrylate (PEGDA, average Mn 600, CAS: 26570–48–9, RYOJI), Calcium chloride ($CaCl_2$, ≥96.0%, CAS: 10043–52–4) were bought from Shanghai Aladdin Bio-Chem Technology Co, China. Nanoclay (Nanomer® PGV, ≥96.0%, CAS: 1332–58–7) was obtained from Nanocor company, China. The PGV nanoclay consisted of silicates nanoplates of 2 to hundred nm thickness (average lengths are up to 16–22 μm and the average interplanar spacing is 1.2–1.4 nm). Water was ultrapure grade supplied from a Milli-Q purification system (Millipore, USA).

2.2. Bacterial strains and growth media

The heterotrophic bacterium (*Oceanimonas* sp. XH2) with ammonia removal capability was isolated from a wastewater treatment plant in Xiamen City. The 16S rRNA gene sequence for the strain *Oceanimonas* sp. XH2 has been submitted to the NCBI GenBank database with the accession number MZ956164. The culture medium and the bacterial morphology of the strain are available in Supplementary Information Text S1 and Fig. S1, respectively. Ammonia was quantified according to the method of a previous study [30].

2.3. Preparation of PEGDA-Alginate-PVA-Nanoclay (PAPN) bio-ink

Sodium alginate and PVA are biopolymers with good biocompatibility and water solubility [31]. The none crosslinking PVA can be easily dissolved in water to further improve the porous structure of 3D bio-scaffold, which will facilitate diffusion of the medium to support the nutrients to the bacteria. In the batch ammonia removal experiments, all laboratory glassware and deionized (DI) water were autoclaved before being used in the experiments and all operations were carried out in a super-clean bench (Lichen equipment Co., Ltd, China). Sodium alginate-PVA solution was prepared with sodium alginate (5 wt%) and PVA (5 wt%) in deionized (DI) water at 80 °C. PEGDA was mixed with DI water (20 wt%) to prepare PEGDA-nanoclay suspension. The PEGDA-nanoclay suspensions were prepared as follows: adding different amounts of nanoclay (0, 3, 5, 7 wt%) to the DI water, followed by adding PEGDA solution homogenized at 250×g for 5 min using a solder paste mixer (ZYMC-200, Shenzhen ZYE Technology Co., Ltd). Sodium alginate-PVA and PEGDA-nanoclay solutions were mixed in a 1:1 (v:v) ratio, and the mixed solution was allowed to homogenize overnight. Afterwards, this pre-gel solution was mixed and equilibrated for 5 min in a vacuum chamber for degassing. Subsequently, water-soluble VA-086 was added to the pre-gel solution as the photoinitiator.

The bacteria were grown in the culture medium for 48 h and centrifuged at 7500×g for 5 min, and then the supernatant was discarded. For the control groups, harvested bacteria were inactivated under sterilization at 121 °C for 30 min. After preparation of bacteria samples, approximately 0.1 g (wet weight) bacteria pellet was transferred into 10 mL PEGDA-Alginate-PVA-Nanoclay (PAPN) pre-gel solution and mixed thoroughly for the experiment groups. After completing all the above steps, the PAPN bio-ink was obtained. The final bacterial cell concentration was 1.2×10^3 CFU/g bio-ink. The compositions of the PEGDA-Alginate-PVA-Nanoclay (PAPN) bio-ink are shown in Table S1.

All laboratory glassware and deionized (DI) water were autoclaved before being used in the experiments, and all operations were carried out on a super-clean bench (Lichen Equipment Co., Ltd, China).

2.4. Fabrication of PAPN 3D bio-scaffold

3D printed hydrogel scaffolds (15 mm × 15 mm × 5 mm) were fabricated using a custom-made 3D bioprinter platform equipped with a blue LED lamp under a 405 nm wavelength (Fig. S2). During printing, each layer was illuminated for 23 s and a total of 10 min. The printed model is shown in Fig. S3. The PAPN bio-ink was loaded into the printing carriage of material extrusion (MEX) 3D bioprinter for extrusion through a 21 G flat tip needle (diameter=0.4 mm), under air pressure 0.7 MPa, the speed of needle 200 mm s^{-1}, the printed layer thickness 0.4 mm, and the printing process was performed at 30 °C. Following extrusion, printed shapes were placed in blue LED light (405 nm wavelength, 55 W cm^{-2}) to complete the covalent crosslinking of the PEGDA polymer chains. After the printing process, alginate is further ionically crosslinked in the presence of $CaCl_2$ solution (4 wt%) at room temperature for 30 min for ion exchange, which imparts stiffness into the network.

2.5. Characterization of the mechanical and physicochemical properties

Rheology and Photorheology tests were performed at 30 °C using a rheometer (DHR-2, TA instruments, USA), employing steel-made parallel geometries (ϕ = 25 mm), and the gap between the parallel was 300.0 μm. The shear rate ranged from 0.01 to 100 s^{-1}. The photorheology of the PAPN ink was measured with a 25 mm UV curable parallel plate. The UV LED (5 mW cm^{-2}) was turned on at the 20th s, and the test procedure was for another 100 s

After curing, the tensile and compressive properties of hydrogel were measured using a universal testing machine (AGX-100 plus, Shimadzu, Japan) at a compression rate of 5 mm min^{-1}. Uniaxial tensile tests were conducted according to the method reported by Zhang et al. [32] and performed on dog-bone-shaped samples with a length a_0 = 45 mm, a width b_0 = 20 mm, and a thickness t_0 = 1.5 mm (Fig. S4) at a speed of 5 mm min^{-1}. Compression tests used samples with a size of 10 mm × 10 mm × 5 mm. All the tests were performed with triplicate independent experiments. The Fourier-transform infrared spectroscopy (FT-IR) analysis was performed by an attenuated total reflection Nicolet iS5 spectrometer (Thermo Fisher Scientific, USA) in the range of 400–4000 cm^{-1} at a 4 cm^{-1}.

2.6. Structural characterization and bacteria viability assessment

For scanning electron microscopy (SEM) analysis of the scaffolds and bacterial morphology during the nitrification process, all the samples were fixed with 2.5% glutaraldehyde in 0.1 M phosphate-buffered saline (PBS, pH 7.0) for 6 h and dehydrated in graded ethanol solution with increasing concentrations of 50%, 70%, 80%, 90%, and 100%. After dehydration, the samples were dried by freeze-drying and observed using a scanning electron microscope (S-4800, Hitachi, Japan). Furthermore, Leica DM2700M light microscope (Leica Microsystems GmbH, Wetzlar, Germany) was employed to observe 3D bio-scaffolds porosity without freeze-drying. The surface area pore size distribution of the PAPN 3D bio-scaffold sample was measured by an Autosorb iQ_2 analyzer (Quantachrome Instruments, Boynton Beach, USA) using the freeze-dried sample.

Bacteria in PAPN 3D bio-scaffold were stained using the LIVE/DEAD® BacLight™ Bacterial Viability kits (Invitrogen, Carlsbad, CA) to evaluate the bacteria viability. After staining, the samples were observed by Zeiss LSM710 confocal laser scanning microscope (Zeiss, Oberkochen, Germany) (excitation: 488 nm; emission: 543 nm).

2.7. Experimental setup

2.7.1. The batch ammonia removal experiments

The batch experiment was performed in the flasks filled with 50 mL synthetic wastewater (NH_4^+-N = 70 and 200 mg L^{-1}, Text S1) and 5 g of the PAPN 3D bio-scaffold, and operated per 72 h for one cycle over 216 h to confirm the stable function of PAPN 3D bio-scaffold (Fig. S5). The experimental setup is shown in Table S1.

To verify the functional stability of the PAPN 3D bio-scaffold, the bio-scaffolds were stored without medium at room temperature for 168 h. Afterwards, those bio-scaffolds were used to test the ammonia removal efficiency. The whole experiments including experiment (active bacteria) and control (dead bacteria) groups was performed at 30 °C with triplicate independent experiments.

2.7.2. Quantitative analysis

Samples (1 mL) for quantitative analysis were taken per 12 h from the flasks. Quantitative analysis of ammonia was performed by using a UV–visible spectrophotometer (PerkinElmer, Lambda 950, Waltham, MA, USA) according to the method of the previous study [30,33] (Text S2). The growth of bacteria in the liquid synthetic wastewater was monitored by measuring the optical density at 600 nm (OD_{600}).

Subsequently, cell proliferation in the PAPN 3D bio-scaffold was analyzed following the process described below. Firstly, the scaffold was homogenized into 10 mL PBS (0.1 M, pH 7.0) using a glass homogenizer and serially diluted using 1 mL PBS. Then 50 μL of each diluted suspension was plated on LB agar plates, incubated at 30 °C for 24 h, and the number of colonies was counted. The dilution factor was used to calculate the colony forming units (CFUs) per gram for each PAPN 3D bio-scaffold.

2.8. Statistical analysis

The removal efficiency "R" is calculated by Eq. (1).

$$R(\%) = \frac{(C_0 - C_t)}{C_0} x100\% \quad (1)$$

Here, C_0 and C_t are the initial and at any time "t" concentrations of ammonia (mg/L), respectively. R is the removal efficiency.

All Data represent at least three independent experiments (n = 3) and are presented as means and standard errors.

3. Results and discussion

3.1. 3D printing strategy of dual crosslinked hydrogel scaffolds with complex architecture using PEGDA-Alginate-PVA-Nanoclay (PAPN) bio-ink

PEGDA is a synthetic material with good water-solubility and can achieve crosslinking reactions at a specific wavelength of light [34,35]. The hydrogel material made from PEGDA has a compression modulus similar to that of human cartilage tissue and therefore, has a good application prospect in bioengineering [36]. The hydrogel formed after PEGDA curing has a smooth surface and is easy to lose water but not easy to absorb proteins [37], resulting in poor cell adsorption [38] and poor porosity and connectivity at the microscale. For this reason, the combination of sodium alginate, a naturally biocompatible polymer, provides a substratum that promotes microbial growth, leading to increased microbial cell viability [39,40]. By combining PEGDA, alginate, PVA, and nanoclay, we obtained biomaterial ink with high viscosity because smectite nanoclay is self-assembled through electrostatic interactions to form a gel when in static equilibrium [28].

The schematic illustration of the overall fabrication process of PAPN bio-ink into a 3D scaffold is shown in Scheme 1. During the printing process, the PAPN bio-ink (Scheme 1 (A)) was then extruded through a 21 G needle to form a hydrogel filament. Due to the thixotropic

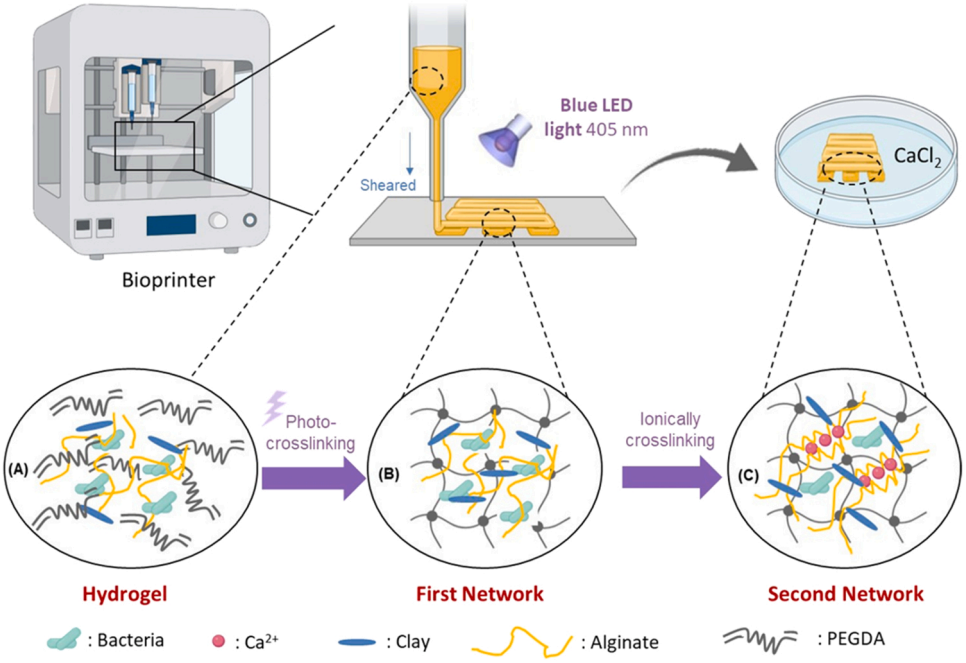

Scheme 1. Schematic illustration of material extrusion-based 3D printing PAPN bio-ink into bio-scaffold.

properties of PAPN bio-ink, there was a change from a solid-like state into a sol state, resulting in low viscosity ink easily extruded from the nozzle [28]. After extrusion, the bio-ink rapidly transformed into the hydrogel state after the release of shear stress, thus forming a stable hydrogel filament construction. Secondly, the 3D scaffold was printed in a layer-by-layer approach by stacking the filament, and the PEGDA within the filament was crosslinked to the first network by photo-crosslinking of the methacrylate groups with the application of the 405 nm blue light and a nontoxic photoinitiator VA-086 [41–43], then resulting in a stable scaffold (Scheme 1 (B) and Fig. S6 (a)).

Afterwards, the printed scaffolds were soaked in 4 wt% $CaCl_2$ solutions for ionic crosslinking of alginate (Scheme 1 (C)). During this process, a second crosslinked network was generated by combining macromers alginate with Ca^{2+} ions (Fig. S6 (b)). Fig. 1(a) shows a 3D printed grid scaffold with 26 layers using 2.5 wt% nanoclay with PAPN bio-ink. Most of previous research about immobilized bacteria used sodium alginate and PVA as the materials and showed the disadvantages such as poor stability, easy particle breakage and low mechanical strength [10,44]. Benefiting from the dual crosslinked network, which can ensure the stability, the scaffold exhibits deformation recovery ability essential for its practical application (Fig. 1(b, c)).

3.2. *Rheological behaviors and optimization of PAPN bio-ink*

The MEX 3D printing requires that the ideal ink should be shear thinning inside the extrusion needle and quickly return to its original

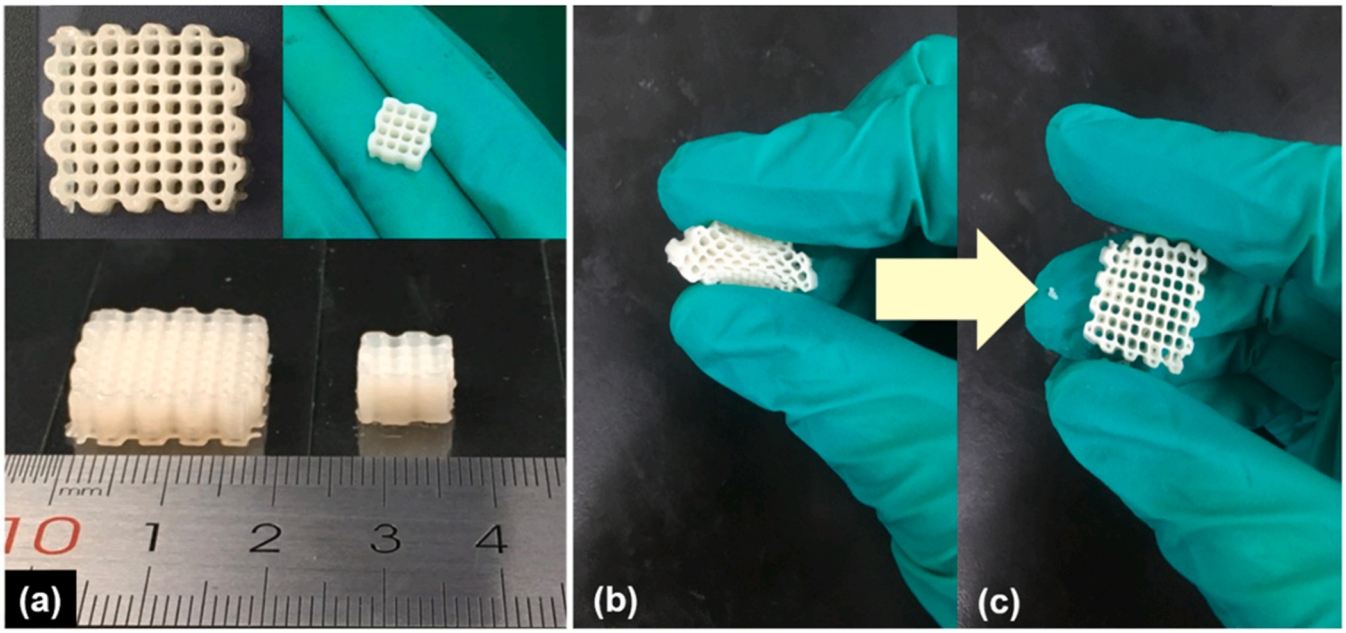

Fig. 1. Photographs of the 3D printing bio-scaffold samples.

viscosity upon exiting. To investigate the printability of the PAPN bio-ink, the rheological properties were evaluated. Previous studies revealed that nanoclay was an effective filler for increasing the viscosity without compromising the hydrogel's adsorption potential [28,45,46]. In the designs of the bio-ink, four different concentrations of nanoclay (0 wt%, 1.5 wt%, 2.5 wt%, and 3.5 wt%) were used to evaluate the effect of nanoclay on the rheology characteristics. After the addition of 0 wt%, 1.5 wt%, 2.5 wt% and 3.5 wt% nanoclay in the PAPN ink, it can be seen in Fig. 2(a) that different concentrations of nanoclay in the ink showed different flow behaviors. Quantitatively, Fig. 2(b) shows that as the nanoclay concentration increased from 0 wt% to 3.5 wt%, the viscosity of the PAPN ink gradually increased from 12.6 to 2949 ± 0.8 Pa.s at the low shear rate of 10^{-2} s^{-1}, and 1.0–3.8 ± 0.3 Pa.s at high shear rates of 10^{2} s^{-1}, and the ink containing 2.5 wt% and 3.5 wt% nanoclay had a comparable viscosity. As the shear rate increased, the PAPN ink showed shear-thinning behavior. The increase in the shear rate broke the interaction between the macromolecular chains in the PAPN ink, causing the viscosity to decline and making ink easy to extrude [47,48]. After extrusion without the influence of shear pressure, the macromolecular chains of the ink re-entangled, and the viscosity returned to its original level [49].

In addition, the storage modulus (G') and loss modulus (G'') of the PAPN ink was measured by the angular frequency (0.1–100 rad s^{-1}) function, as shown in Fig. 2(c). Moreover, the storage and loss moduli increased with the addition of nanoclay from 1.5 wt% to 3.5 wt%. The storage modulus was higher than the loss modulus ($G' > G''$), which displayed the characteristics of a solid-like response within this range [50,51]. Based on the result, the amount of nanoclay in the ink that impacts the viscosity and the structure of the PAPN hydrogel properties can be identified. Adding 2.5 wt% and 3.5 wt% nanoclay results in similar rheology properties. Furthermore, Gao et al. [28] have shown that nanoclay was favorable for the growth of microbes. However, the increase in nanoclay amount may affect cell bioactivity. For this reason, in this study, adding 2.5 wt% nanoclay would be suitable for the PAPN bio-ink in our experiments.

Photorheology probed the photocuring kinetics of PAPN ink. Fig. 2 (d) depicts typical photocuring behavior, including storage modulus (G') and loss modulus (G'') of the PAPN ink under photo-irradiation, measured upon applying the oscillatory strain. In the experiments, samples showed a crossover of the storage and loss modulus ($G' > G''$) photocuring with 23 s, and G' quickly plateaued upon light irradiation through the quartz parallel plate. The photocuring time of this study was shorter than the previous study [15], which used 365 nm UV light to crosslink under 60 s irradiation. The shorter photocuring time will reduce UV light exposure of bio-scaffolds and will be beneficial for increasing the viability of microorganisms.

Through the above rheology analysis of PAPN ink, we have determined the printing parameters, and the ink exhibits favorable 3D printability. Controlling the concentration of nanoclay in the ink permits the viscosity to be optimized for MEX-based printing while still maintaining 3D structures without requiring supporting material. We have demonstrated the PAPN ink can also be printed into various 3D shapes free from vertical limitations (Fig. S7).

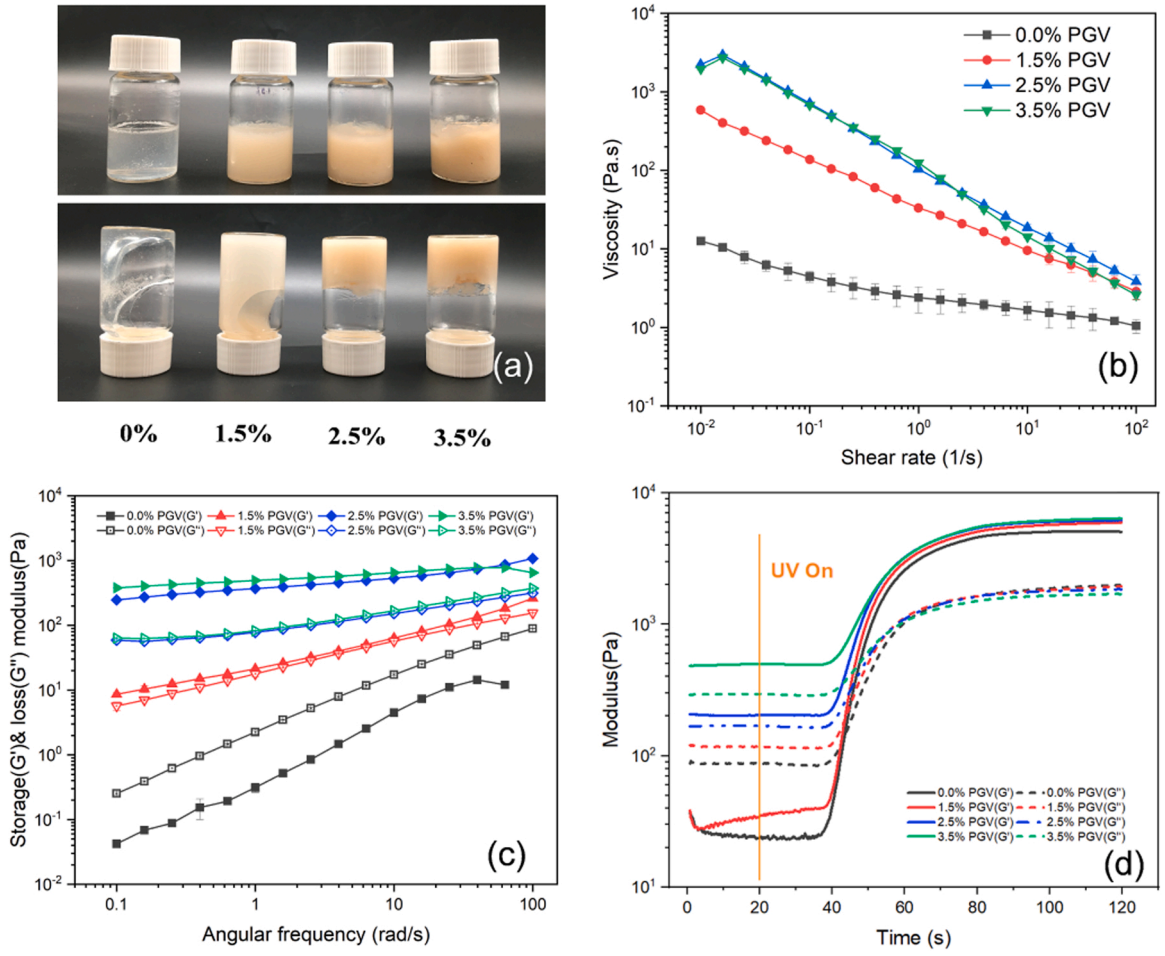

Fig. 2. Rheological running of PAPN bio-ink characterization, n = 3. (a) Rheological properties of the PAPN bio-ink within four different concentrations of nanoclay; (b) Apparent viscosity as a function of shear rate; (c) Shear storage and loss modulus; (d) Photorheology for neat PAPN bioink, depicting storage (G') and loss (G'') modulus increase as a function of UV exposure time (on at 20 s).

3.3. Mechanical and FT-IR characterization of PAPN 3D bio-scaffolds

The FT-IR analysis was subsequently carried out to verify the PAPN bio-ink crosslinking process with different crosslinking methods (photo-crosslinking, ionic crosslinking, and dual crosslinking) as shown in Fig. 3 (a). The characteristic absorption peaks 810, 1190, and 1410 cm^{-1} for double bonds in acrylate groups disappeared after photo-crosslinking [52]. Moreover, the absorption peak 1450 cm^{-1} was observed, which presents the -CH_2 asymmetric stretching vibration. The results showed that PEGDA was crosslinked during the photocuring. The near UV photoinitiator VA-086 generated radicals to initiate the acrylate monomer polymerization of the PEGDA to form a crosslinking network (Fig. S6 (a)), converting PEGDA solution into PEG gel with a network structure[53].

The effect of the crosslinking method of PAPN bio-ink on mechanical characterization has been tested by the compressive\tensile stress-strain. Fig. 3(b, c) presents compressive and tensile stress-strain curves of the PAPN hydrogel using three crosslinking methods (photo-crosslinking, Ca^{2+} ionic crosslinking, and dual-crosslinking), which mainly exhibited linear stress-strain behavior. The results showed the tensile strength increased from 15.4 ± 0.1 kPa (ionic crosslinking), 104.8 ± 0.9 kPa (photo-crosslinking) to 185.8 ± 0.7 kPa (dual crosslinking). The elongation at break of ionic crosslinking, photo-crosslinking and dual crosslinking increased from 4.6%, 16.8–22.9%, respectively (Fig. 3(b)). Moreover, the compressive test displayed the dual crosslinking sample (365.2 ± 0.3 kPa) had a higher compressive strength than single crosslinking samples (ionic crosslinking 176.8 ± 0.3 kPa and photo-crosslinking 273.4 ± 0.6 kPa), and the compressive strength of the dual crosslinking sample improved about 106.5% compared to the ionic crosslinking sample (Fig. 3(c)).

Alginate is a nontoxic, biodegradable, and biocompatible natural source of polymer and is often applied as the material for encapsulation and immobilization of microbes by ionic crosslinking [54]. However, the ionically crosslinked alginate hydrogels showed weak mechanical strength and low elasticity [55]. The non-cytotoxic PEGDA, which can be photo-crosslinked [56], has been used to improve the mechanics of the PAPN 3D bio-scaffolds. From the tensile stress-strain and compressive strength test results, the ultimate strength and compression modulus increased by photo-crosslinking combined with ionic crosslinking. The dual crosslinking method increases the mechanical and structural stability of the 3D printed bio-scaffold.

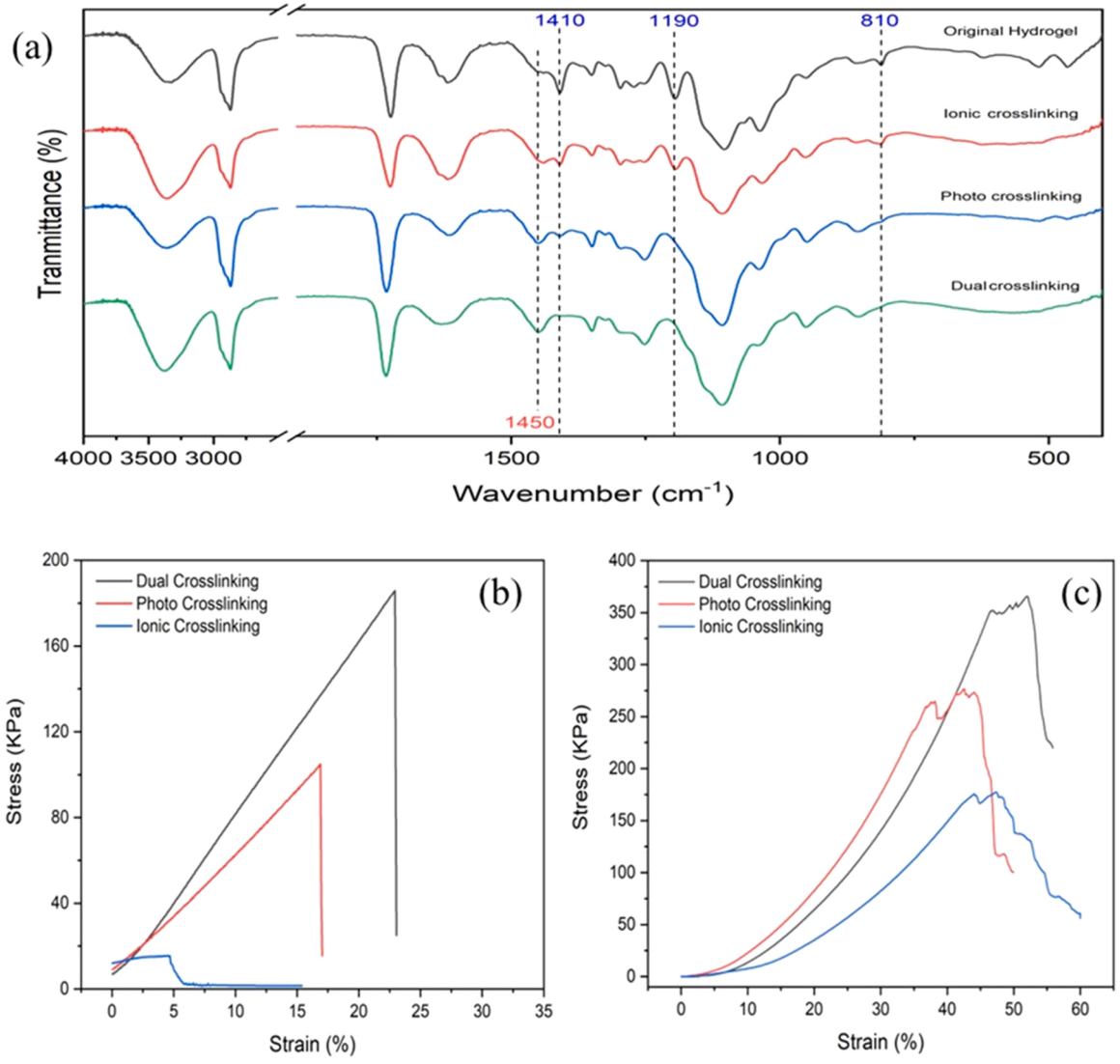

Fig. 3. (a) The FT-IR spectra for the different crosslinking methods; Mechanical strength characterization (n = 3): (b) the tensile stress-strain and (c) the compressive stress-strain curves of the PAPN 3D printed scaffolds.

3.4. Morphology and viability of bacteria in the PAPN 3D bio-scaffolds

A high-resolution scanning electron microscope was used to characterize the morphologies of freeze-dried scaffolds (Fig. 4). It can be clearly seen that the 3D printed grid-like scaffold morphologies showed relatively dense and rough surface structure (Fig. 4(a) and Fig. S8). The SEM and light microscope results revealed that PAPN 3D bio-scaffold had porous structures inside with encapsulated bacteria (Fig. 4(b) and Fig. S8, S9). Therefore, the bio-scaffolds exhibited permeability of water/nutrients due to their porous structure, providing the water and nutrients for the encapsulated bacteria to grow. Pores inside the 3D bio-scaffolds may allow bacteria proliferation, migration, and interaction with neighboring bacteria depending on their physical locations and the secretory molecules surrounding them [57]. In addition, the pore size distribution in Fig. S10 shows that a number of mesoporous pores (2–50 nm) were presented on the surface of the 3D bio-scaffold, which can be attributed to the filling of nanoparticles[28] and PVA [58]. Brunauer-Emmett-Teller (BET) N_2 adsorption/desorption isotherm analysis showed a surface area of 10.0 m^2/g and an average pore diameter of 2.77 nm.

Interestingly, after 168 h of incubation, the microtopography of the scaffold showed some irregular and rough surfaces (Fig. 4(c) and Fig. S10, S11), with a surface area of 15.27 m^2/g, and an average pore diameter of 4.57 nm. Meanwhile, Fig. S11 shows that there were pores with a pore size of 1–5 μm inside the 3D structure. The FT-IR spectra showed that the typical absorption peak of 3380 cm^{-1} for PVA disappeared after 168 h of incubation (Fig. S12). Accordingly, the results suggested that PVA was likely diffused from the scaffold into the medium, increasing the surface area porosity and growth space for bacteria and promoting the mass transfer performance in the 3D bio-scaffold. Our results agreed with the observation of previous studies [58–60].

Bacterial viability to evaluate the biocompatibility of the 3D bio-scaffolds was investigated and visualized through LIVE/DEAD® BacLight™ Bacterial Viability kits staining using the confocal laser scanning microscope. The green color represents live bacteria while dead or inactive bacterial cells with compromised membrane show red color. High bacteria viability was seen in the beginning and after the substrate was depleted, more cell decay was observed at 168 h of incubation (Fig. 5). In addition, cell proliferation analysis was further confirmed through the plate count method. In the beginning, bacterial cells in the bio-scaffold were around 1.2×10^3 CFU/g. After 1 day, cell numbers increased to 1.4×10^7 CFU/g and further grew to 2.0×10^{12} CFU/g after 7 days (Fig. S13), which suggested bacteria in the 3D bio-scaffold maintained proliferation through 7-day culturing period. The increase of bacterial cell numbers was also consistent with the images of bacterial viability results (Fig. 5) and SEM results (Fig. 4(b) and (d)), which implied the whole 3D printing process was under mild conditions (room temperature, 405 nm, and no toxic organic solvent) and combination of ionic crosslinking and photo-crosslinking process was not harmful to the majority of bacteria [61]. Previous studies also suggested that the photoinitiator, which does not require UV irradiation, e.g. VA086, showed better biocompatibility and more suitable for 3D bioprinting [42,62,63]. Hence, our PAPN 3D printed bio-scaffold is proven to be beneficial for producing immobilized microbial inocula and effective for the application of functional bacteria.

3.5. Ammonia removal capabilities of the functional PAPN 3D bio-scaffolds

The removal of different initial NH_4^+-N concentrations (70 and 200 mg L^{-1}) was measured at the temperature of 30 °C with an incubation time of 84 h to evaluate the function of the PAPN 3D bio-scaffolds. As shown in Fig. 6(a), the low initial NH_4^+-N concentration (70 mg L^{-1}) group more rapidly showed high removal efficiency. It could be distinctly observed that for the high initial NH_4^+-N concentration group (200 mg L^{-1}) there was a lag phase of NH_4^+-N removal, and the removal rate increased after 24 h until it reached the stable stage at 72 h. The lag phase in the early stage should be owing to the lower cell numbers of *Oceanimonas* sp. XH2 in the bio-scaffolds. The continuously increased removal rate of ammonia could be attributed to the increase in *Oceanimonas* sp. XH2 cells (Fig. S13 and S14). Similarly, previous study mentioned PVA-sodium alginate gel bead embedding can maintain the

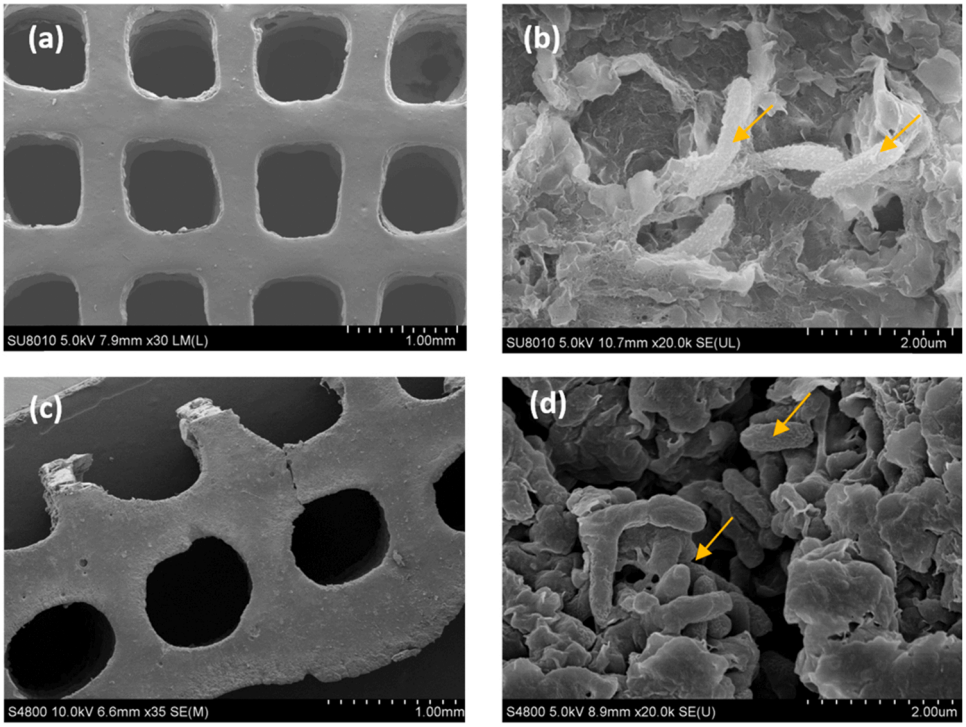

Fig. 4. Scanning electron microscopy (SEM) images of immobilized microbial 3D bio-scaffold during the experiment period; (a) 0 h sample's surface; (b) 0 h sample's inside; (c) 168 h sample's surface; (d) 168 h sample's inside. Yellow arrows indicate *Oceanimonas* sp. XH2 bacterial cells.

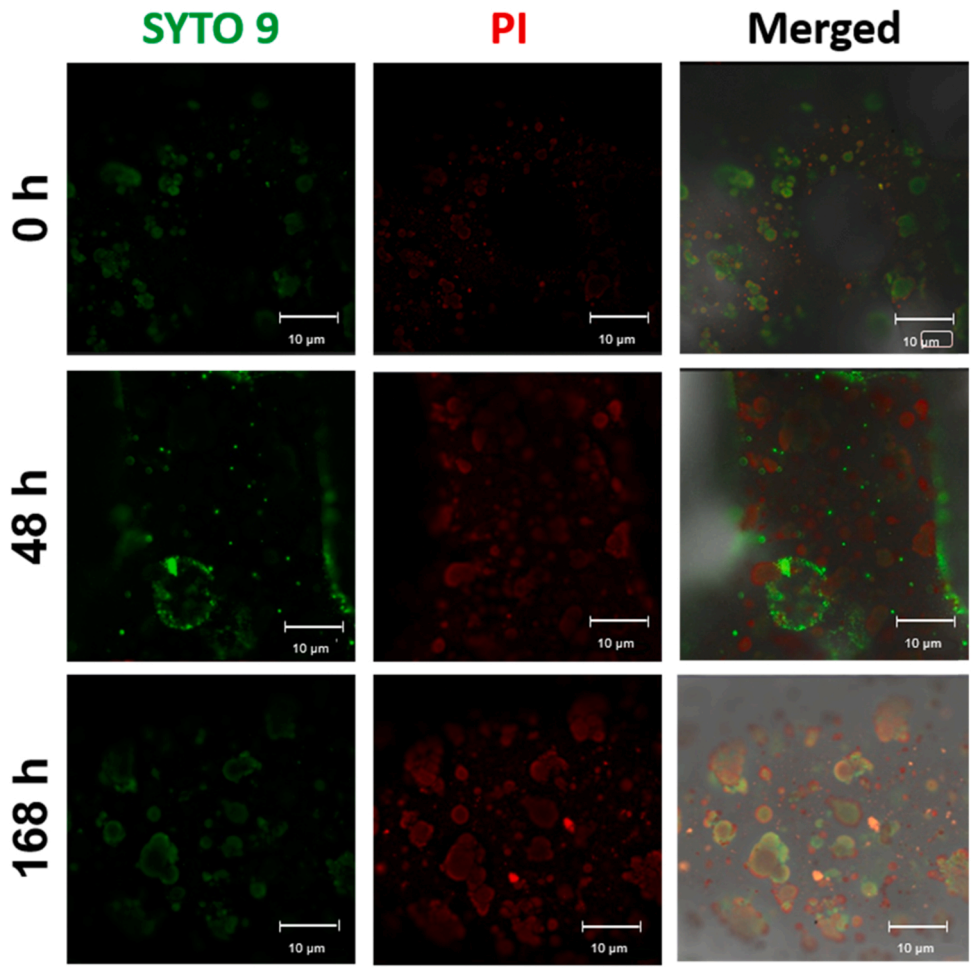

Fig. 5. The bacterial viability of 3D printing bio-scaffold. Living cells are depicted in green and dead cells are in red. The scale bar is 10 μm.

growth and activity of bacteria [64,65]. On the other hand, as Fig. S14 and previous literature revealed, bacteria could be released in the culture medium, possibly due to the increased bacterial population and the diffusion of bacteria from the porous hydrogel scaffolds [66]. Therefore, PAPN 3D bio-scaffolds could also act as an inoculant to release bacteria and remove ammonia in the medium. In our study, we compared the performance of 3D bio-scaffolds and suspended bacteria as shown in Fig. S15. As the results shown in Fig. S15, the ammonia removal efficiency was comparable between 3D bio-scaffolds and suspended bacteria.

Furthermore, to validate the stability of the PAPN 3D bio-scaffolds, ammonia removal rates were repeated over 3 cycles of 216 h. As shown in Fig. 6(b) and Fig. S16, the removal rate increased from the first cycle to the third cycle, with the complete removal time from 60 h to 12 h. The improved ammonia removal performance is hypothesized to be caused by the gradual increase of the *Oceanimonas* sp. XH2 bacterial cell numbers (shown in Fig. S13 and S14). The results illustrate that the densely embedded bio-scaffolds can provide a durable and stable living environment for the bacteria, and thereby promote ammonia removal.

We further took the bio-scaffolds out of the culture medium and stored them at room temperature to simulate the transportation environment without low temperature and culture medium for 168 h. Subsequently, we tested the removal efficacy of the PAPN 3D bio-scaffolds. Fig. 6(c) demonstrated that the bio-scaffolds still showed high performance in removing ammonia, compared with the original PAPN 3D bio-scaffolds. The degradation curves showed that approximately 96.2 ± 1.3% of the low concentration ammonia (NH_4^+-N = 70 mg L^{-1}) was removed in the first 12 h, and 25 ± 0.1% was removed for the high concentration ammonia (NH_4^+-N = 200 mg L^{-1}). The moisture content of the 3D bio-scaffolds was 76.2 ± 1.6% after the material was placed at room temperature for 168 h, corresponding to the water content loss only about 3.4 ± 0.3% (Fig. S17). The 3D bio-scaffolds can provide a suitable environment for the growth of bacteria and preserve bacteria while retaining microbial viability and activity during room temperature storage. Our results demonstrated 3D bio-scaffolds had a high potential for long-distance transport of bacteria for wastewater treatment, which was also supported by the previous study of 3D printed bio-scaffolds using different material [67]. Therefore, when compared with previous immobilized bacteria for ammonia removal using alginate and PVA [31,68], our prepared PAPN 3D bio-scaffolds have demonstrated superior reusability and stability, indicating the potential for future applications.

4. Conclusion

In this research, a novel visible-light-based PAPN bio-ink was successfully established for applying 3D printing technology to immobilize microorganisms. The printability of the PAPN bio-ink hydrogel material was enhanced by adding nanoclay, and the viscosity of 2.5% nanoclay in the PAPN bio-ink was optimized for MEX-based printing. One heterotrophic bacterium (*Oceanimonas* sp. XH2) with ammonia removal ability was successfully immobilized in the 3D printed bio-scaffolds with satisfactory cell viability and excellent capacity of ammonia removal in the solution. Repeated use of bio-scaffolds has shown enhanced ammonia removal efficiency due to bacterial cell proliferation within the hydrogel scaffolds. The 3D bio-scaffold maintained ammonia

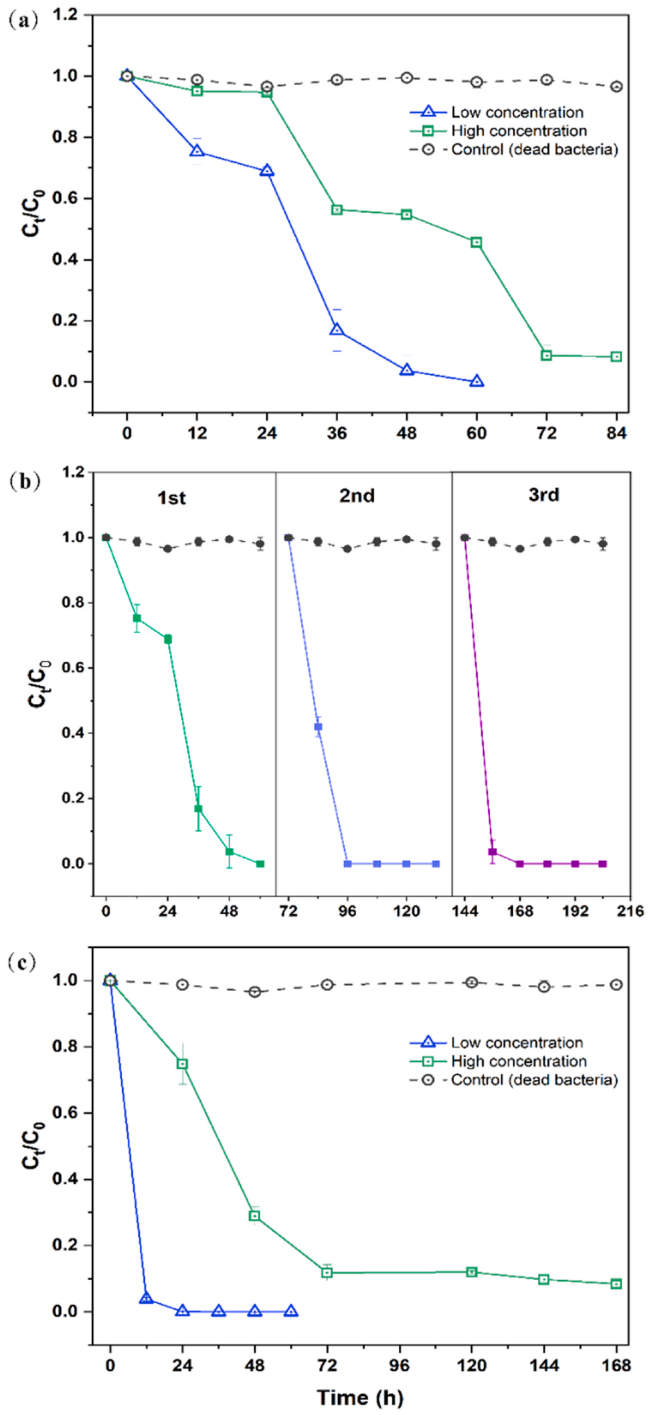

Fig. 6. The ammonia nitrogen removal performance over the whole study period (n = 3): (a) removal rate of different ammonia concentrations; (b) stable efficacy during reuse recycles; (c) removal efficiency after stored in simulated transportation environment for 168 h. The low and high concentrations of NH_4^+-N were 70 and 200 mg L^{-1}, respectively.

removal capability after 168-hour storage without medium under room temperature. Viability results and SEM images demonstrated that the majority of bacteria were active and present in the porous structures of 3D bio-scaffolds after printing. Moreover, the mechanical strength of 3D printed bio-scaffolds was achieved using dual crosslinking, including the photo-crosslinking under 405 nm visible-light irradiation and the ionic crosslinking using calcium ions. Our work demonstrates the PAPN dual crosslinking method in 3D printing to immobilize heterotrophic bacteria with ammonia removal ability for wastewater treatment. The advanced 3D printing technology along with dual crosslinking methods has shown the potential to produce stable encapsulated functional bacteria with various 3D structures which can be preserved and reused in environmental remediation.

CRediT authorship contribution statement

Yan Li: Writing – original draft, Validation, Methodology, Conceptualization. **Zixiang Weng:** Methodology, Data curation. **Dan Qin:** Methodology, Investigation. **Kunrong Li:** Investigation, Formal analysis. **Shuqiang Peng:** Validation, Software, Methodology, Formal analysis. **Chang-ping Yu:** Writing – review & editing, Supervision, Funding acquisition, Conceptualization. **Lixin Wu:** Writing – review & editing, Supervision, Funding acquisition, Conceptualization. **Longhui Zheng:** Methodology. **Jiangwei Li:** Methodology.

Declaration of Competing Interest

The authors declare that they have no known competing financial interests or personal relationships that could have appeared to influence the work reported in this paper.

Data Availability

Data will be made available on request.

Acknowledgements

We appreciated Miss. Tian Yuan Chen, Miss. Xiaoxuan Liang and Fuyi Huang for the instrument analysis guidance. This work was funded by National Natural Science Foundation of China (Grant No.: 52102148), the Major Science and Technology Project of Fujian Province (Grant No.: 2021HZ027003), the FJIRSM and IUE Joint Research Fund (Grant No.: RHZX-2019-005), the Science and Technology Planning Project of Fuzhou City of Fujian Province (Grant No.: 2020-C-141) and Scientific Research Foundation of Fujian University of Technology (Project No.: GY-Z20083).

Appendix A. Supporting information

Supplementary data associated with this article can be found in the online version at doi:10.1016/j.addma.2022.103268.

References

[1] Q.H. Zhang, W.N. Yang, H.H. Ngo, W.S. Guo, P.K. Jin, M. Dzakpasu, S.J. Yang, Q. Wang, X.C. Wang, D. Ao, Current status of urban wastewater treatment plants in China, Environ. Int. 92–93 (2016) 11–22.
[2] Z. Yang, J. Xia, L. Zou, Y. Qiao, S. Xiao, Y. Dong, C. Liu, Efficiency and driving force assessment of an integrated urban water use and wastewater treatment system: Evidence from spatial panel data of the urban agglomeration on the middle reaches of the Yangtze River, Sci. Total Environ. 805 (2022), 150232.
[3] X. Zhou, R. Luo, L. Yao, S. Cao, S. Wang, B. Lev, Assessing integrated water use and wastewater treatment systems in China: A mixed network structure two-stage SBM DEA model, J. Clean. Prod. 185 (2018) 533–546.
[4] A. Saravanan, P. Senthil Kumar, S. Jeevanantham, S. Karishma, B. Tajsabreen, P. R. Yaashikaa, B. Reshma, Effective water/wastewater treatment methodologies for toxic pollutants removal: processes and applications towards sustainable development, Chemosphere 280 (2021), 130595.
[5] P.Y. Nguyen, G. Carvalho, M.A.M. Reis, A. Oehmen, A review of the biotransformations of priority pharmaceuticals in biological wastewater treatment processes, Water Res. 188 (2021), 116446.
[6] N.Y. Donkadokula, A.K. Kola, I. Naz, D. Saroj, A review on advanced physico-chemical and biological textile dye wastewater treatment techniques, Rev. Environ. Sci. Bio/Technol. 19 (3) (2020) 543–560.
[7] A.S. Oberoi, Y. Jia, H. Zhang, S.K. Khanal, H. Lu, Insights into the fate and removal of antibiotics in engineered biological treatment systems: a critical review, Environ. Sci. Technol. 53 (13) (2019) 7234–7264.
[8] H.A. Ahmad, S.-Q. Ni, S. Ahmad, J. Zhang, M. Ali, H.H. Ngo, W. Guo, Z. Tan, Q. Wang, Gel immobilization: a strategy to improve the performance of anaerobic ammonium oxidation (anammox) bacteria for nitrogen-rich wastewater treatment, Bioresour. Technol. 313 (2020), 123642.

[9] H. Bae, M. Choi, C. Lee, Y.-C. Chung, Y.J. Yoo, S. Lee, Enrichment of ANAMMOX bacteria from conventional activated sludge entrapped in poly(vinyl alcohol)/sodium alginate gel, Chem. Eng. J. 281 (2015) 531–540.
[10] Q. Chang, A. Ali, J. Su, Q. Wen, Y. Bai, Z. Gao, R. Xiong, Efficient removal of nitrate, manganese, and tetracycline by a polyvinyl alcohol/sodium alginate with sponge cube immobilized bioreactor, Bioresour. Technol. 331 (2021), 125065.
[11] P.-H. Wu, T.-M. Hsieh, H.-Y. Wu, C.-P. Yu, Characterization of the immobilized algae-based bioreactor with external ceramic ultrafiltration membrane to remove nutrients from the synthetic secondary wastewater effluent, Int. Biodeterior. Biodegrad. 164 (2021), 105309.
[12] S.C.D. Sharma, J. Li, A. Hu, C.-C. Chang, C.-P. Yu, Integration of pre-colonized and mediator immobilized mixed culture for the improvement of electricity production of microbial fuel cells, Environ. Technol. Innov. 22 (2021), 101514.
[13] C. Ma, D. Qin, Q. Sun, F. Zhang, H. Liu, C.P. Yu, Removal of environmental estrogens by bacterial cell immobilization technique, Chemosphere 144 (2016) 607–614.
[14] P.-H. Wu, Y.-C. Cheng, H.-Y. Chen, T.-w Chueh, H.-C. Chen, L.-H. Huang, Z.-X. Wu, T.-M. Hsieh, C.-C. Chang, P.-Y. Yang, C.-F. Lin, C.-P. Yu, Using the entrapped bioprocess as the pretreatment method for the drinking water treatment receiving eutrophic source water, Environ. Pollut. 248 (2019) 57–65.
[15] M. Schaffner, P.A. Ruhs, F. Coulter, S. Kilcher, A.R. Studart, 3D printing of bacteria into functional complex materials, Sci. Adv. 3 (12) (2017) eaao6804.
[16] S. Kyle, 3D printing of bacteria: the next frontier in biofabrication, Trends Biotechnol. 36 (4) (2018) 340–341.
[17] X. Wang, M. Jiang, Z. Zhou, J. Gou, D. Hui, 3D printing of polymer matrix composites: A review and prospective, Composites Part B: Engineering 110 (2017) 442–458.
[18] J. Caro-Astorga, K.T. Walker, N. Herrera, K.Y. Lee, T. Ellis, Bacterial cellulose spheroids as building blocks for 3D and patterned living materials and for regeneration, Nat. Commun. 12 (1) (2021) 5027.
[19] J.L. Connell, E.T. Ritschdorff, M. Whiteley, J.B. Shear, 3D printing of microscopic bacterial communities, Proc. Natl. Acad. Sci. USA 110 (46) (2013) 18380–18385.
[20] B.A.E. Lehner, D.T. Schmieden, A.S. Meyer, A straightforward approach for 3D bacterial printing, ACS Synth. Biol. 6 (7) (2017) 1124–1130.
[21] B. Kaczmarek, K. Nadolna, A. Owczarek, The physical and chemical properties of hydrogels based on natural polymers, in: Y. Chen (Ed.), Hydrogels Based on Natural Polymers, Elsevier, 2020, pp. 151–172.
[22] O. Jeon, K.H. Bouhadir, J.M. Mansour, E. Alsberg, Photocrosslinked alginate hydrogels with tunable biodegradation rates and mechanical properties, in: Biomaterials, 30, 2009, pp. 2724–2734.
[23] S. Nagarajan, H. Belaid, C. Pochat-Bohatier, C. Teyssier, I. Iatsunskyi, E. Coy, S. Balme, D. Cornu, P. Miele, N.S. Kalkura, V. Cavaillès, M. Bechelany, Design of boron nitride/gelatin electrospun nanofibers for bone tissue engineering, ACS Appl. Mater. Interfaces 9 (39) (2017) 33695–33706.
[24] T. Mehrotra, S. Dev, A. Banerjee, A. Chatterjee, R. Singh, S. Aggarwal, Use of immobilized bacteria for environmental bioremediation: a review, J. Environ. Chem. Eng. 9 (5) (2021), 105920.
[25] L.E. de-Bashan, Y. Bashan, Immobilized microalgae for removing pollutants: review of practical aspects, Bioresour. Technol. 101 (6) (2010) 1611–1627.
[26] M.C. Arno, M. Inam, A.C. Weems, Z. Li, A.L.A. Binch, C.I. Platt, S.M. Richardson, J. A. Hoyland, A.P. Dove, R.K. O'Reilly, Exploiting the role of nanoparticle shape in enhancing hydrogel adhesive and mechanical properties, Nat. Commun. 11 (1) (2020) 1420.
[27] A. Chang, N. Babhadiashar, E. Barrett-Catton, P. Asuri, Role of nanoparticle–polymer interactions on the development of double-network hydrogel nanocomposites with high mechanical strength, Polymers 12 (2) (2020) 470.
[28] Q. Gao, X. Niu, L. Shao, L. Zhou, Z. Lin, A. Sun, J. Fu, Z. Chen, J. Hu, Y. Liu, Y. He, 3D printing of complex GelMA-based scaffolds with nanoclay, Biofabrication 11 (3) (2019), 035006.
[29] A. Pourjavadi, M. Doroudian, A. Ahadpour, S. Azari, Injectable chitosan/kappa-carrageenan hydrogel designed with au nanoparticles: a conductive scaffold for tissue engineering demands, Int J. Biol. Macromol. 126 (2019) 310–317.
[30] J. Wu, Y. Hong, F. Guan, Y. Wang, Y. Tan, W. Yue, M. Wu, L. Bin, J. Wang, J. Wen, A rapid and high-throughput microplate spectrophotometric method for field measurement of nitrate in seawater and freshwater, Sci. Rep. 6 (2016) 20165.
[31] Y. Dong, Y. Zhang, B. Tu, Immobilization of ammonia-oxidizing bacteria by polyvinyl alcohol and sodium alginate, Braz. J. Microbiol. 48 (2017) 515–521.
[32] B. Zhang, S. Li, H. Hingorani, A. Serjouei, L. Larush, A.A. Pawar, W.H. Goh, A. H. Sakhaei, M. Hashimoto, K. Kowsari, S. Magdassi, Q. Ge, Highly stretchable hydrogels for UV curing based high-resolution multimaterial 3D printing, J. Mater. Chem. B 6 (20) (2018) 3246–3253.
[33] S. Ringuet, L. Sassano, Z.I. Johnson, A suite of microplate reader-based colorimetric methods to quantify ammonium, nitrate, orthophosphate and silicate concentrations for aquatic nutrient monitoring, J. Environ. Monit. 13 (2) (2011) 370–376.
[34] P.J. Stahl, T.R. Chan, Y.I. Shen, G. Sun, S. Gerecht, S.M. Yu, Capillary network-like organization of endothelial Cells in PEGDA scaffolds encoded with angiogenic signals via triple helical hybridization, Adv. Funct. Mater. 24 (21) (2014) 3213–3225.
[35] V.B. Morris, S. Nimbalkar, M. Younesi, P. McClellan, O. Akkus, Mechanical properties, cytocompatibility and manufacturability of chitosan:PEGDA hybrid-gel scaffolds by stereolithography, Ann. Biomed. Eng. 45 (1) (2017) 286–296.
[36] V. Chan, J.H. Jeong, P. Bajaj, M. Collens, T. Saif, H. Kong, R. Bashir, Multi-material bio-fabrication of hydrogel cantilevers and actuators with stereolithography, Lab Chip 12 (1) (2012) 88–98.
[37] J.H. Lee, H.B. Lee, J.D. Andrade, Blood compatibility of polyethylene oxide surfaces, Prog. Polym. Sci. 20 (6) (1995) 1043–1079.
[38] J. Zhu, Bioactive modification of poly(ethylene glycol) hydrogels for tissue engineering, Biomaterials 31 (17) (2010) 4639–4656.
[39] M. Roy, K. Devoe, A. Bandyopadhyay, S. Bose, Mechanical and in vitro biocompatibility of brushite cement modified by polyethylene glycol, Mater. Sci. Eng. C Mater. Biol. Appl. 32 (8) (2012) 2145–2152.
[40] L. Wang, R.M. Shelton, P.R. Cooper, M. Lawson, J.T. Triffitt, J.E. Barralet, Evaluation of sodium alginate for bone marrow cell tissue engineering, Biomaterials 24 (20) (2003) 3475–3481.
[41] A.D. Rouillard, C.M. Berglund, J.Y. Lee, W.J. Polacheck, Y. Tsui, L.J. Bonassar, B. J. Kirby, Methods for photocrosslinking alginate hydrogel scaffolds with high cell viability, Tissue Eng. Part C. Methods 17 (2) (2011) 173–179.
[42] W.T. Han, T. Jang, S. Chen, L.S.H. Chong, H.D. Jung, J. Song, Improved cell viability for large-scale biofabrication with photo-crosslinkable hydrogel systems through a dual-photoinitiator approach, Biomater. Sci. 8 (1) (2019) 450–461.
[43] L.H. Kang, P.A. Armstrong, L.J. Lee, B. Duan, K.H. Kang, J.T. Butcher, Optimizing Photo-Encapsulation Viability of Heart Valve Cell Types in 3D Printable Composite Hydrogels, Ann. Biomed. Eng. 45 (2) (2017) 360–377.
[44] F. Li, W.-j Mao, X. Li, X.-y Wang, Z.-h Xiao, Y.-y Zhou, G.-m Zeng, Characterization of Microcystis aeruginosa immobilized in complex of PVA and sodium alginate and its application on phosphorous removal in wastewater, J. Cent. South Univ. 22 (1) (2015) 95–102.
[45] T. Ahlfeld, G. Cidonio, D. Kilian, S. Duin, A.R. Akkineni, J.I. Dawson, S. Yang, A. Lode, R.O.C. Oreffo, M. Gelinsky, Development of a clay based bioink for 3D cell printing for skeletal application, Biofabrication 9 (3) (2017), 034103.
[46] M. Bhatia, S.B. Rajulapati, S. Sonawane, A. Girdhar, Synthesis and implication of novel poly(acrylic acid)/nanosorbent embedded hydrogel composite for lead ion removal, Sci. Rep. 7 (1) (2017) 16413.
[47] Y. Gao, X. Jin, Dual crosslinked methacrylated alginate hydrogel micron fibers and tissue constructs for cell biology, Mar. Drugs 17 (10) (2019).
[48] J. Yin, M. Yan, Y. Wang, J. Fu, H. Suo, 3D bioprinting of low-concentration cell-laden gelatin methacrylate (GelMA) bioinks with a two-step cross-linking strategy, ACS Appl. Mater. Interfaces 10 (8) (2018) 6849–6857.
[49] S. Huan, B.D. Mattos, R. Ajdary, W. Xiang, L. Bai, O.J. Rojas, Two-phase emulgels for direct ink writing of skin-bearing architectures, Adv. Funct. Mater. 29 (40) (2019).
[50] S.M. Mihaila, A.K. Gaharwar, R.L. Reis, A.P. Marques, M.E. Gomes, A. Khademhosseini, Photocrosslinkable kappa-carrageenan hydrogels for tissue engineering applications, Adv. Health Mater. 2 (6) (2013) 895–907.
[51] S.H. Hsiao, S.H. Hsu, Synthesis and characterization of dual stimuli-sensitive biodegradable polyurethane soft hydrogels for 3D cell-laden bioprinting, ACS Appl. Mater. Interfaces 10 (35) (2018) 29273–29287.
[52] Z. Wang, H. Ma, B.S. Hsiao, B. Chu, Nanofibrous ultrafiltration membranes containing cross-linked poly(ethylene glycol) and cellulose nanofiber composite barrier layer, Polymer 55 (1) (2014) 366–372.
[53] W. Zhou, H. Zhang, Y. Liu, X. Zou, J. Shi, Y. Zhao, Y. Ye, Y. Yu, J. Guo, Preparation of calcium alginate/polyethylene glycol acrylate double network fiber with excellent properties by dynamic molding method, Carbohydr. Polym. 226 (2019), 115277.
[54] E. Sanchez-Rexach, T.G. Johnston, C. Jehanno, H. Sardon, A. Nelson, Sustainable materials and chemical processes for additive manufacturing, Chem. Mater. 32 (17) (2020) 7105–7119.
[55] J.-Y. Sun, X. Zhao, W.R.K. Illeperuma, O. Chaudhuri, K.H. Oh, D.J. Mooney, J. J. Vlassak, Z. Suo, Highly stretchable and tough hydrogels, Nature 489 (7414) (2012) 133–136.
[56] C. Warr, J.C. Valdoz, B.P. Bickham, C.J. Knight, N.A. Franks, N. Chartrand, P. M. Van, Ry, K.A. Christensen, G.P. Nordin, A.D. Cook, Biocompatible PEGDA resin for 3D printing, ACS Appl. Bio Mater. 3 (4) (2020) 2239–2244.
[57] S.R. Batool, M.A. Nazeer, D. Ekinci, A. Sahin, S. Kizilel, Multifunctional alginate-based hydrogel with reversible crosslinking for controlled therapeutics delivery, Int J. Biol. Macromol. 150 (2020) 315–325.
[58] Y. Luo, G. Luo, M. Gelinsky, P. Huang, C. Ruan, 3D bioprinting scaffold using alginate/polyvinyl alcohol bioinks, Mater. Lett. 189 (2017) 295–298.
[59] C.-Y. Huang, K.-H. Hu, Z.-H. Wei, Comparison of cell behavior on pva/pva-gelatin electrospun nanofibers with random and aligned configuration, Sci. Rep. 6 (1) (2016) 37960.
[60] L. Pang, Y. Shen, H. Hu, X. Zeng, W. Huang, H. Gao, H. Wang, D. Wang, Chemically and physically cross-linked polyvinyl alcohol-borosilicate gel hybrid scaffolds for bone regeneration, Mater. Sci. Eng.: C. 105 (2019), 110076.
[61] O. Jeon, J.-Y. Shin, R. Marks, M. Hopkins, T.-H. Kim, H.-H. Park, E. Alsberg, Highly elastic and tough interpenetrating polymer network-structured hybrid hydrogels for cyclic mechanical loading-enhanced tissue engineering, Chem. Mater. 29 (19) (2017) 8425–8432.
[62] Z. Wang, X. Jin, R. Dai, J.F. Holzman, K. Kim, An ultrafast hydrogel photocrosslinking method for direct laser bioprinting, RSC Adv. 6 (25) (2016) 21099–21104.
[63] J. Colle, P. Blondeel, A. De Bruyne, S. Bochar, L. Tytgat, C. Vercruysse, S. Van Vlierberghe, P. Dubruel, H. Declercq, Bioprinting predifferentiated adipose-derived mesenchymal stem cell spheroids with methacrylated gelatin ink for adipose tissue engineering, J. Mater. Sci.: Mater. Med. 31 (4) (2020) 36.
[64] L. Zhang, S. Okabe, Rapid cultivation of free-living planktonic anammox cells, Water Res. 127 (2017) 204–210.
[65] M. Ali, S. Okabe, Anammox-based technologies for nitrogen removal: advances in process start-up and remaining issues, Chemosphere 141 (2015) 144–153.

[66] Y. Bashan, Alginate beads as synthetic inoculant carriers for slow release of bacteria that affect plant growth, Appl. Environ. Microbiol. 51 (5) (1986) 1089–1098.

[67] K. Li, Y. Li, J. Hu, Y. Zhang, Z. Yang, S. Peng, L. Wu, Z. Weng, Waterborne polyurethane acrylates preparation towards 3D printing for sewage treatment, Materials 15 (9) (2022) 3319.

[68] Y. Dong, Y. Zhang, B. Tu, J. Miao, Immobilization of ammonia-oxidizing bacteria by calcium alginate, Ecol. Eng. 73 (2014) 809–814.